Integrated Systems and Technologies

Cancer Research

Enhanced Detection of Cancer Biomarkers in Blood-Borne Extracellular Vesicles Using Nanodroplets and Focused Ultrasound

Robert J. Paproski[1,5], Juan Jovel[2,3], Gane Ka-Shu Wong[2,3,4], John D. Lewis[5], and Roger J. Zemp[1]

Abstract

The feasibility of personalized medicine approaches will be greatly improved by the development of noninvasive methods to interrogate tumor biology. Extracellular vesicles shed by solid tumors into the bloodstream have been under recent investigation as a source of tumor-derived biomarkers such as proteins and nucleic acids. We report here an approach using submicrometer perfluorobutane nanodroplets and focused ultrasound to enhance the release of extracellular vesicles from specific locations in tumors into the blood. The released extracellular vesicles were enumerated and characterized using micro flow cytometry. Only in the presence of nanodroplets could ultrasound release appreciable levels of tumor-derived vesicles into the blood. Sonication of HT1080-GFP tumors did not increase the number of circulating tumor cells or the metastatic burden in the tumor-bearing embryos. A variety of biological molecules were successfully detected in tumor-derived extracellular vesicles, including cancer-associated proteins, mRNAs, and miRNAs. Sonication of xenograft HT1080 fibrosarcoma tumors released extracellular vesicles that contained detectable RAC1 mRNA with the highly tumorigenic N92I mutation known to exist in HT1080 cells. Deep sequencing serum samples of embryos with sonicated tumors allowed the identification of an additional 13 known heterozygous mutations in HT1080 cells. Applying ultrasound to HT1080 tumors increased tumor-derived DNA in the serum by two orders of magnitude. This work is the first demonstration of enhanced extracellular vesicle release by ultrasound stimulation and suggests that nanodroplets/ultrasound offers promise for genetic profiling of tumor phenotype and aggressiveness by stimulating the release of extracellular vesicles. *Cancer Res; 77(1); 3–13. ©2016 AACR.*

Introduction

Circulating tumor cells, extracellular vesicles (EV), and free-circulating DNA and RNA are promising sources of tumor biomarkers that could provide diagnostic and prognostic information important for personalized medicine (1–6). Despite progress in detecting circulating tumor cells (CTC), existing assays still have low sensitivity due to the reduced number of CTCs often found in patients' blood (1–10 CTC/mL).

EVs, which include exosomes, apoptotic bodies, and other vesicles, are typically between 30 and 2,000 nm in diameter and are naturally released from normal and cancerous cells (7). EV release is involved in various physiological processes including cell–cell communication and apoptosis (7). Cancer cells have been shown to shed large numbers of these vesicles compared with noncancerous cells (8). Cell surface proteins can be found on their surface, and cytoplasmic molecules including proteins, mRNA, and miRNA can be found inside EVs, suggesting that they contain many of the potential biomarkers found in intact cells (9). EVs in blood have thus been under intense investigation as a source of biomarkers for various diseases including cancer (10, 11). As a source of biomarkers, EVs may have some advantages compared to non-encapsulated nucleic acid biomarkers as vesicle-encapsulated biomarkers are likely to be protected against degradation. Furthermore, tumor-shed vesicles are far more abundant than circulating tumor cells, which should allow for more sensitive detection of circulating biomarkers. Recently, circulating vesicles containing high levels of glypican-1 identified pancreatic ductal adenocarcinoma in 190 cancer patients with 100% sensitivity and specificity demonstrating the diagnostic potential of EVs (12). Prostate cancer–specific mRNA biomarkers PCA-3 and TMPRSS2:ERG have recently been shown to be detected in exosomes in urine and blood (13).

Free-circulating and vesicle-encapsulated DNA and RNA offer considerable potential for genetic diagnostics of tumors. In particular, detection of tumor-specific mutations have yet to be widely explored, yet could open up new opportunities for genetic profiling. Unfortunately, such DNA and RNA fragments from host tumors are not always abundant in blood.

Ultrasound has been demonstrated to enhance the release of various biomarkers from cancer cells (14–16). D'Souza and

[1]Department of Electrical and Computer Engineering, University of Alberta, Edmonton, Alberta, Canada. [2]Department of Biological Sciences, University of Alberta, Edmonton, Alberta, Canada. [3]Department of Medicine, University of Alberta, Edmonton, Alberta, Canada. [4]BGI-Shenzhen, Beishan Industrial Zone, Yantian District, Shenzhen, China. [5]Department of Oncology, University of Alberta, Edmonton, Alberta, Canada.

Note: Supplementary data for this article are available at Cancer Research Online (http://cancerres.aacrjournals.org/).

Corresponding Authors: Roger J. Zemp, University of Alberta, Donadeo ICE 13-340, Edmonton, Alberta T6G 2V4, Canada. Phone: 780-492-1825; Fax: 780-492-1811; E-mail: rzemp@ualberta.ca; and John D. Lewis, University of Alberta, 5-142C Katz Group Building, 114th Street and 87th Avenue, Edmonton, Alberta T6G 2E1, Canada. Phone: 780-492-6113; Fax: 780-492-8160; jdlewis@ualberta.ca

colleagues showed that sonication of LS174T xenograft tumors in mice increased blood levels of carcinoembryonic antigen protein compared with pre-ultrasound levels (14). Furthermore, sonication of breast cancer ZR-75-1 cells in tissue culture enhanced the release of nucleic acids including mammary-specific mammaglobin mRNA and miR21-5p, a miRNA found overexpressed in many cancers (15). This suggests that many different cell-derived biomarkers can be liberated from cells using ultrasound, yet the principle challenge for this approach is that ultrasound alone releases relatively low levels of biomarkers from cancer cells (15, 16). Ultrasound contrast agents such as microbubbles and nanodroplets have been demonstrated to enhance the biomarker-releasing effects of ultrasound (15, 16). Microbubbles, which typically are 1 to 4 μm perfluorocarbon gas bubbles with a phospholipid or polymer shells, can undergo cavitation and highly energetic destruction when exposed to high pressure ultrasound (>1 MPa peak negative pressure), which can alter membrane permeability of nearby cells (17, 18). Phase-change nanodroplets are similar to microbubbles but typically have a liquid perfluorocarbon core and are less than a micrometer in diameter (19). High pressure ultrasound can induce nanodroplets to phase change into microbubbles, which can subsequently be destroyed with ultrasound (20). Nanodroplets and microbubbles perform similarly in cell culture for the enhancement of ultrasound-mediated biomarker release (16).

Cancer cells exposed to ultrasound in the presence of microbubbles display substantial deformation of the plasma membrane (21). This suggests that the enhanced release of biomarkers may be due in part to the enhanced release of EVs. The impact of nanodroplets/microbubbles and ultrasound on the release of biomarker-bearing EVs and free-circulating DNA/RNA *in vivo* has yet to be investigated.

We hypothesized that exposing tumors to high intensity focused ultrasound in the presence of nanodroplets would amplify the release of EVs carrying relevant tumor-specific biomarkers into adjacent blood vessels (Fig. 1). To test this, we exposed HT1080-GFP tumors in chicken embryos to nanodroplets/ultrasound and analyzed serum EVs using micro flow cytometry, real-time PCR, and deep sequencing. We demonstrate for the first time

that nanodroplets and focused ultrasound stimulate the release of large numbers of EVs from tumor cells into the bloodstream, allowing enhanced detection of relevant protein, mRNA, miRNA, and DNA biomarkers containing tumor-specific mutations that may be of great diagnostic value.
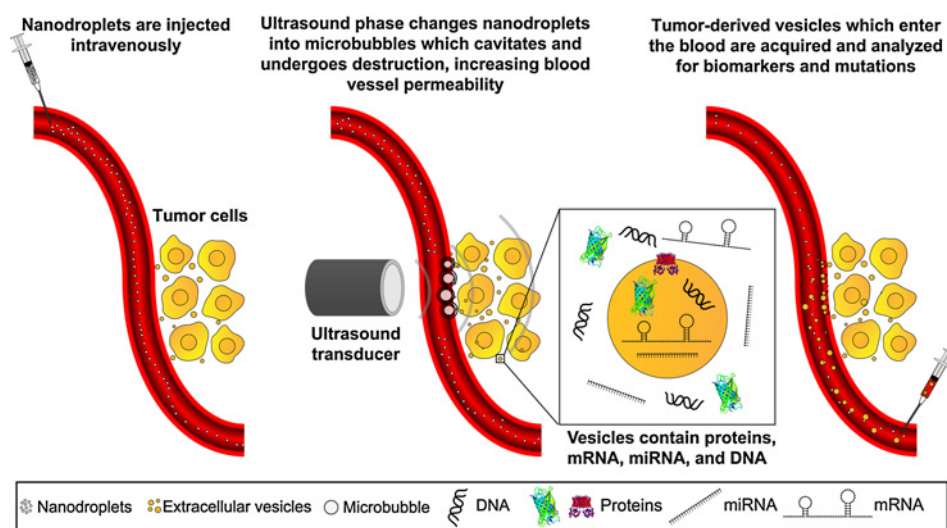
Materials and Methods

Ultrasound system used for vesicle release

The electronic signal from a Tektronix AFG 3021B function generator was amplified by an Electronics & Innovation 2100L power amplifier, which powered a Sonic Concepts H134 MR-006 focused transducer (43-mm diameter). The H134 transducer has a center frequency of 1.15 MHz and a focal depth of 36.5 mm from the transducer housing. The ultrasound beam focal width and length are 1.2 and 8.1 mm, respectively. A custom acrylic water coupling cone was created to allow efficient transmission of ultrasound from the transducer to target cells. Ultrasound pressures were verified using an Onda HN needle hydrophone.

Preparation and characterization of perfluorobutane nanodroplets

A phospholipid stock containing 1,2-dipalmitoyl-*sn*-glycero-3-phosphocholine (0.4 mg/mL), 1,2-dipalmitoyl-*sn*-glycero-3-phosphate (0.045 mg/mL), and 1,2-dipalmitoyl-*sn*-glycero-3-phosphoethanolamine-N-[methoxy(polyethylene glycol)-2000] (0.145 mg/mL; all phospholipids were from Avanti Polar Lipids) were dissolved in PBS containing glycerol (10%, v/v) and propylene glycol (10%, v/v), heated to 85°C for 1 hour, and stored at 4°C. For each batch of nanodroplets, phospholipid stock (1 mL) was aliquoted in a 2 mL vial with septum and the headspace was filled with perfluorobutane (FluoroMed L.P.). The vial was shaken in a VialMix shaker (Bristol Myers Squibb Medical Imaging, Inc.) for 45 seconds to create microbubbles. Microbubbles were centrifuged at 400 × g for 4 minutes and the floating microbubbles were washed once with 1 mL PBS with 10% (v/v) glycerol and 10% (v/v) propylene glycol. These washed microbubbles were used as ultrasound contrast agents for some experiments. To create nanodroplets, the vial containing washed microbubbles had approximately 10 mL of room air injected through the

Figure 1.
Overview of ultrasound-mediated tumor EV release. Before tumor sonication, nanodroplets are injected intravenously. High pressure ultrasound is applied to tumor cells that phase changes nanodroplets into microbubbles that are subsequently destroyed in highly energetic reactions that increases vascular permeability and stimulates EV release from tumor cells. Some tumor-derived EVs enter the vasculature and are acquired from the blood and are characterized to profile the sonicated tumor for biomarkers.

septum using a 10 mL syringe and 27 gauge needle. The pressurized vial caused the microbubbles to phase-change into nanodroplets, which were used for subsequent experiments. Microbubble conversion efficiency was determined using a Z2 Coulter Counter. For characterization experiments (NanoSight and cryo-TEM imaging), 100 μL nanodroplets were layered on top of 200 μL 25% (w/v) sucrose (density 1.1 g/cm^3) and samples were centrifuged at $16,160 \times g$ for 5 minutes. Lipid particles without liquid perfluorobutane cores remained above the sucrose whereas nanodroplets formed a pellet below the sucrose. The nanodroplet pellets were resuspended in PBS and nanodroplets size and concentration were characterized using a NanoSight LM10 system. Cryo-transmission electron microscopy was also performed for visualization of the sucrose-purified nanodroplets (see Supplementary Materials and Methods).

Vesicle release from HT1080 cells in 96-well plates

The cell lines used in this study were generously provided by Dr. James Quigley (The Scripps Research Institute, La Jolla, CA). HT1080 and HT1080-GFP cells were cultured in high-glucose DMEM with 10% (v/v) FBS. Ninety-six well plates were inoculated with 7,000 cells/well. Two days after cell inoculation, medium in wells were removed and 100 μL fresh medium ± 2% (v/v) nanodroplets was added to each well. Some experiments replaced nanodroplets with 2% sucrose-purified nanodroplets or 2% diluted (0.51%, v/v) microbubbles with a final concentration of approximately 0.01% (v/v). For some wells, focused 1.15 MHz ultrasound (30 MPa pk-pk pressure, 10–10,000 cycles/burst, 1 burst per well) was applied upward from the bottom of the plate through the center of each well using the transducer coupling cone for ultrasound alignment. An Onda HNP needle hydrophone was used to measure pressures inside a well of a 96-well plate. After cell sonication, 60 μL medium from each well was acquired, centrifuged at $2,000 \times g$ for 10 minutes to pellet large debris/cells and 40 μL of supernatant was diluted in 200 μL PBS and analyzed with the Apogee A50 micro flow cytometer. For all flow cytometry experiments, photomultiplier voltage settings for small angle light scatter, large angle light scatter, and 488 nm laser/green filter were 208, 300, and 362, respectively. For all flow cytometry cytograms, data are presented in $\log_{10}$ scales on all axes. Nanosphere polystyrene beads (Thermo Scientific) were also run to approximate sizes of EVs.

Cell viability of sonicated HT1080-GFP cells in 96-well plates

The toxicity of ultrasound/nanodroplets was assessed in cultured HT1080-GFP cells as described in the Supplementary Materials and Methods.

Vesicle release from HT1080 tumors in the chicken embryo

All animal experiments were approved by the University of Alberta's Animal Care and Use Committee Livestock group. Shell-less chicken embryos were prepared as described previously (22). Briefly, fertilized chicken eggs were placed in a humidified 38°C rocking chamber for 3 days followed by cracking of eggs into sterilized plastic weigh boats. The embryos were placed in a 38°C humidified incubator for five days and HT1080 or HT1080-GFP cells were microinjected in the chorioallantoic membrane (CAM; approximately 50,000 cells per injection site; 2–3 injections per chicken embryo). Chicken embryos were placed back in the incubator for 6 days before embryos were used for experiments.

For each chicken embryo, 50 μL nanodroplets, sucrose-purified nanodroplets, microbubbles (0.51%, v/v), or PBS containing glycerol (10%, v/v) and propylene glycol (10%, v/v) was injected intravenously in the CAM. Unless otherwise stated, ultrasound was applied on or away from the tumor approximately 3 minutes after nanodroplet injection and 50 μL blood was sampled thereafter near the sonication site. When no ultrasound was applied to the chicken embryo, blood was sampled near the tumor. Blood was acquired from the chicken embryo by physically disrupting the larger blood vessels in the CAM using a glass needle and collecting blood that pooled on top of the CAM. If ultrasound caused blood to pool on top of the CAM, this blood was taken for analysis. Blood samples were left at room temperature for at least 20 minutes and clotted blood was centrifuged at $2,000 \times g$ for 10 minutes. The supernatant (5 μL serum) was diluted in 295 μL PBS and analyzed with the A50 micro flow cytometer. The gate used to determine GFP$^+$ vesicles was manually drawn to not include events based on cytograms from serum of embryos with sonicated HT1080 tumors (no GFP in these tumors so all vesicles in this sample should not have GFP). This same GFP$^+$ gate was used for *in vitro* experiments described above.

Various experimental parameters were manipulated to identify the optimal conditions for vesicle release from tumors into blood. Unless otherwise stated, ultrasound parameters for tumor sonication were 1.15 MHz, 30 MPa (pk-pk) pressure, 1,000 cycles/burst, 1 burst/seconds, 30 seconds duration. If one parameter was changed, all other parameters remained as described above.

Flow cytometry analysis of HT1080-GFP cells in blood

Chicken embryos bearing HT1080-GFP tumors were injected with nanodroplets and, for some embryos, had tumors sonicated as described above. Blood was collected (50 μL) and was diluted with 50 μL washing buffer, which was PBS containing 3 mg/mL ethylenediaminetetraacetic acid and 2% (v/v) FBS. Some blood samples from embryos without ultrasound exposure had 100,000 HT1080-GFP cells added to the samples to verify HT1080-GFP cells could be isolated and detected by flow cytometry. To separate red blood cells from mono-nuclear cells, diluted blood was layered on top of 200 μL Lymphoprep (STEMCELL Technologies Inc.) in 1.5 mL microcentrifuge tubes and tubes were centrifuged at $800 \times g$ for 20 minutes at room temperature. The mono-nuclear cells at the interface of the solutions were collected, washed with 750 μL washing buffer, and resuspended in 500 μL washing buffer. Cells were analyzed with a BD FACSCanto II flow cytometer and, based on data from samples containing additional HT1080-GFP cells, green fluorescent signal above 10,000 was used as the threshold for identification of HT1080-GFP cells.

Bioluminescence/fluorescence imaging chicken embryo tissues

Chicken embryos bearing a single HT1080-luciferase-GFP tumor were injected intravenously with nanodroplets and had tumors sonicated as described above. Some tumor-bearing embryos did not have nanodroplets injected or tumors sonicated. Four days after ultrasound exposure, embryos were given an intravenous injection of 50 μL luciferin (15 mg/mL) and tissues were dissected from the embryos approximately 3 minutes post-luciferin injection. Dissected tissues included a piece of CAM distant from the primary tumor, liver, lung, and brain, which were rinsed with PBS and stored in 250 μL luciferin (0.3

Paproski et al.

mg/mL). Tissues from individual chicken embryos were imaged for bioluminescence and green fluorescence using a Bruker In-Vivo Xtreme system equipped with a back-illuminated 4 Megapixel camera. Bruker molecular imaging software (version 7.5.2.22464) was used for signal analysis. Bioluminescence signal within tissues was normalized by summing tissue signal, which was divided by tissue weight.

Analysis of GFP mRNA and miR21-5p release from sonicated HT1080 tumors

Chicken embryos bearing HT1080-GFP tumors were injected with nanodroplets and, for some embryos, had tumors sonicated as described above. Serum GFP mRNA and miR21-5p levels were determined as described in the Supplementary Materials and Methods.

Sequencing RAC1 mRNA in HT1080-GFP cell lysates and serum vesicles of chicken embryos with sonicated HT1080-GFP tumors

Chicken embryos bearing HT1080-GFP tumors were injected with nanodroplets and, for some embryos, had tumors sonicated as described above. Serum was collected and processed for RAC1 mRNA sequencing as described in the Supplementary Materials and Methods. The serum RAC1 mRNA sequence was compared with that of cultured HT1080-GFP cell lysates to verify that both sequences matched.

Whole genome sequencing of DNA in serum

Chicken embryos bearing HT1080-GFP or HEp3-GFP tumors were injected with nanodroplets and, for some embryos, tumors were sonicated as described above. Serum was collected

and was processed for whole genome sequencing and analyzed as described in the Supplementary Materials and Methods.
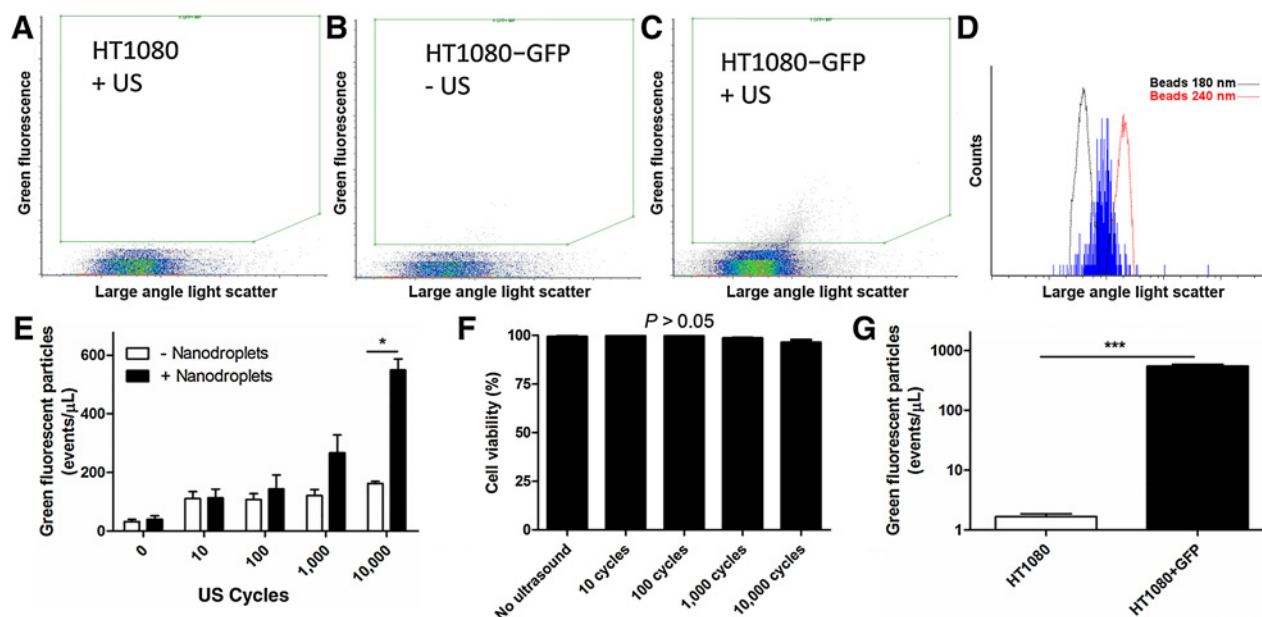
Statistical analysis

Data were analyzed using GraphPad Prism software (version 5.00). For experimental groups where Bartlett test of equal variance provided P values less than 0.05 (i.e., variances were not equal), data were log transformed, which caused Bartlett test P values to be greater than 0.05 (i.e., variances were not different between groups and ANOVA analysis was appropriate). The Student t-test was used when comparing two groups and one-way ANOVA was used when comparing three or more groups. Bonferroni posttest correction was used to compare all pairs of experimental groups and P values ≤ 0.05 were required for statistical significance. For each experiment, the number of samples analyzed per group is described in the figure legends.

Results

Nanodroplets enhance ultrasound-mediated EV release from cancer cells

To determine whether focused ultrasound can stimulate the release of EVs from cancer cells in culture, HT1080-GFP fibrosarcoma cells in 96-well plates were treated with high pressure 1.15 MHz ultrasound and the media was analyzed for EVs using the Apogee A50 micro flow cytometer, which is designed to detect particles as small as 100 nm. The bottom of the plate attenuated approximately 8% of the ultrasound pressure thus cells within the well were exposed to approximately 27.6 MPa pk-pk pressure. Media from HT1080 and HT1080-GFP cells contained very low numbers of green fluorescent EVs (1.7 and 32 vesicles per µL,

Figure 2.
Vesicle release from sonicated HT1080 and HT1080-GFP cells in 96-well plates. **A–C,** Cytograms of green fluorescence and large angle light scatter of vesicles in medium samples from sonicated HT1080 cells (**A**), nonsonicated HT1080-GFP cells (**B**), and sonicated HT1080-GFP cells (**C**). **D,** Histogram of large angle light scatter of green fluorescent positive particles (blue-filled area) from sonicated HT1080-GFP cells, with histograms of reference beads with 180 and 240 nm diameters (black and red traces, respectively). **E,** Green fluorescent particle release from HT1080-GFP cells exposed to different amounts of ultrasound cycles with or without nanodroplets (5 wells per group, *, $P < 0.05$). **F,** Cell viability by Trypan blue staining of HT1080-GFP cells incubated with nanodroplets and exposed to different amounts of ultrasound cycles. **G,** Green fluorescent particle release from sonicated HT1080 and HT1080-GFP cells incubated with nanodroplets (3–5 wells per group).
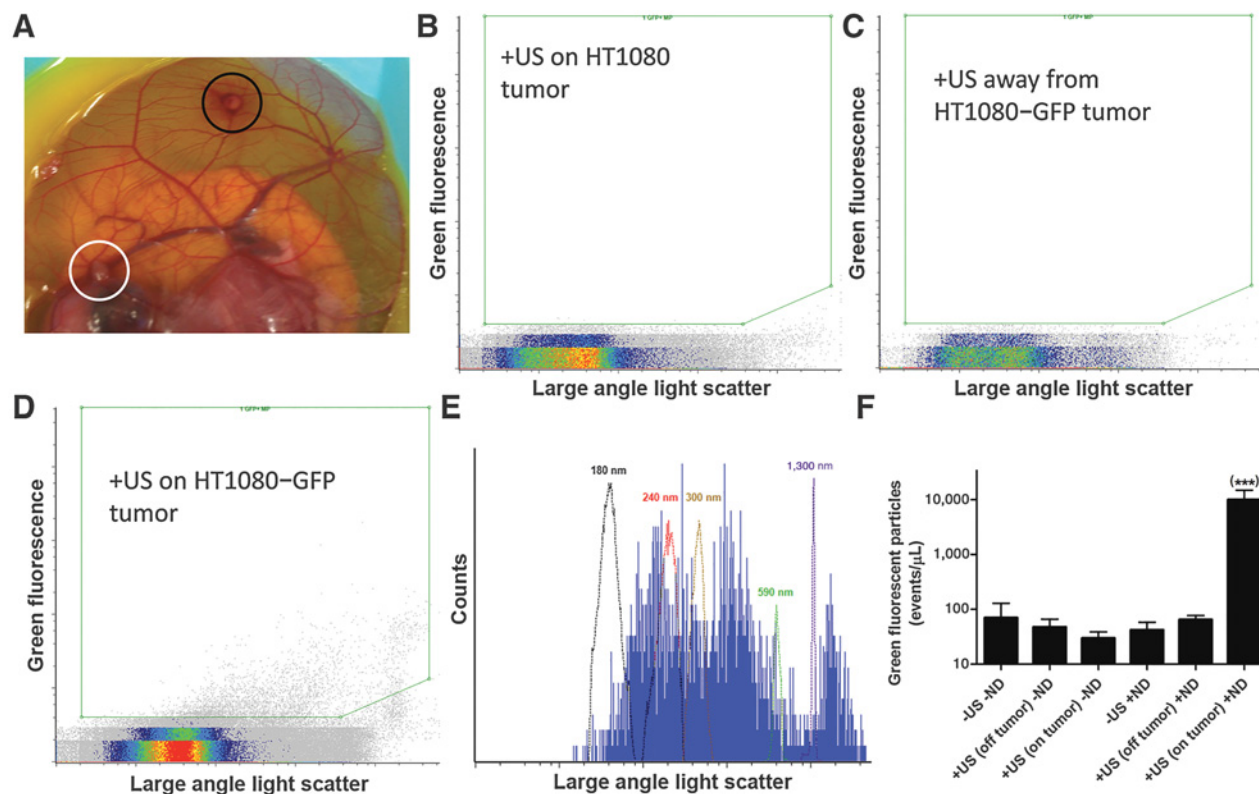
respectively). When 10 to 10,000 cycles of focused ultrasound were applied to HT1080-GFP cells, the level of green fluorescent EVs in the media increased modestly (Fig. 2B, C, E), whereas sonication of HT1080 cells resulted in no significant increase in green fluorescent EVs in the media (Fig. 2A). Comparing the EVs with polystyrene beads of known sizes indicated that the majority of GFP+ EVs were between 180 and 240 nm in diameter (Fig. 2D).

We then investigated the impact of applying focused ultrasound on cultured cells in the presence of perfluorocarbon nanodroplets, which can enhance the effect of ultrasound (Supplementary Fig. S1A). Cryo-electron microscopy imaging of nanodroplets revealed particles between approximately 100–500 nm in diameter (Supplementary Fig. S1B). The nanoparticle tracking analysis method revealed that nanodroplets had a mean diameter of 156 ± 5 nm and a mean concentration of $4.1 \pm 1.0 \times 10^{10}$ particles per mL (Supplementary Fig. S1C). Microscopy imaging of nanodroplet and 4% (v/v) microbubble solutions suggested that nanodroplet solutions without or with sucrose purification had 0.51% and 0.13% of microbubbles remaining in the nanodroplet solutions, respectively (Supplementary Fig. S2). When HT1080-GFP cells were sonicated with 10,000 cycles of ultrasound in the presence of 2% nanodroplets, a significant increase in the number of GFP+ EVs was observed ($P < 0.01$, Fig. 2E)

whereas cell viability did not significantly decrease even at 10,000 cycles of ultrasound (Fig. 2F). Sonication of HT1080-GFP cells with 10,000 cycles of ultrasound with 2% nanodroplets present caused 330-fold greater green fluorescent EV release compared with nonfluorescent HT1080 cells under similar conditions (Fig. 2G). We did observe some cell detachment at the higher ultrasound exposure levels, which likely reflects a limitation in utilizing this technique with cells in two-dimensional (2D) cultures. Nevertheless, these experiments demonstrate that exposing cancer cells to focused ultrasound in the presence of perfluorocarbon nanodroplets significantly increases the release of EVs, which prompted us to investigate whether this could be replicated in an *in vivo* model and whether released EVs could be detected in the bloodstream.

Perfluorobutane nanodroplets required for ultrasound-mediated EV release from tumors

We utilized an *ex ovo* chicken embryo xenograft model where HT1080 or HT1080-GFP tumors are established in the CAM (22–26). Embryos bearing HT1080 and HT1080-GFP tumors were injected intravenously with PBS with or without nanodroplets and were exposed to focused ultrasound on the tumor or on another region of the CAM not containing cancer cells (Fig. 3A).

Figure 3.
Detection of green fluorescent vesicles in serum after intravenous injection of nanodroplets and sonication of HT1080 and HT1080-GFP tumors. **A,** Image of a chicken embryo with a sonicated (black circle) and nonsonicated (white circle) HT1080-GFP tumors after intravenous injection of nanodroplets. **B–D,** Cytograms of green fluorescence and large angle light scatter of particles in the serum of chicken embryos with ultrasound applied on an HT1080 tumor (**B**), ultrasound applied away from an HT1080-GFP tumor (**C**), and ultrasound applied on a HT1080-GFP tumor (**D**). **E,** Histogram of large angle light scatter of green fluorescent positive particles from serum of a chicken embryo with a sonicated HT1080-GFP tumor (blue area). Dashed lines represent histograms of beads with standardized sizes (180, 240, 300, 590, and 1,300 nm). **F,** Serum levels of green fluorescent particles from chicken embryos with or without nanodroplet intravenous injection with or without ultrasound applied on or off HT1080-GFP tumors (5 chicken embryos per group; ***, $P < 0.001$ compared with all other groups).
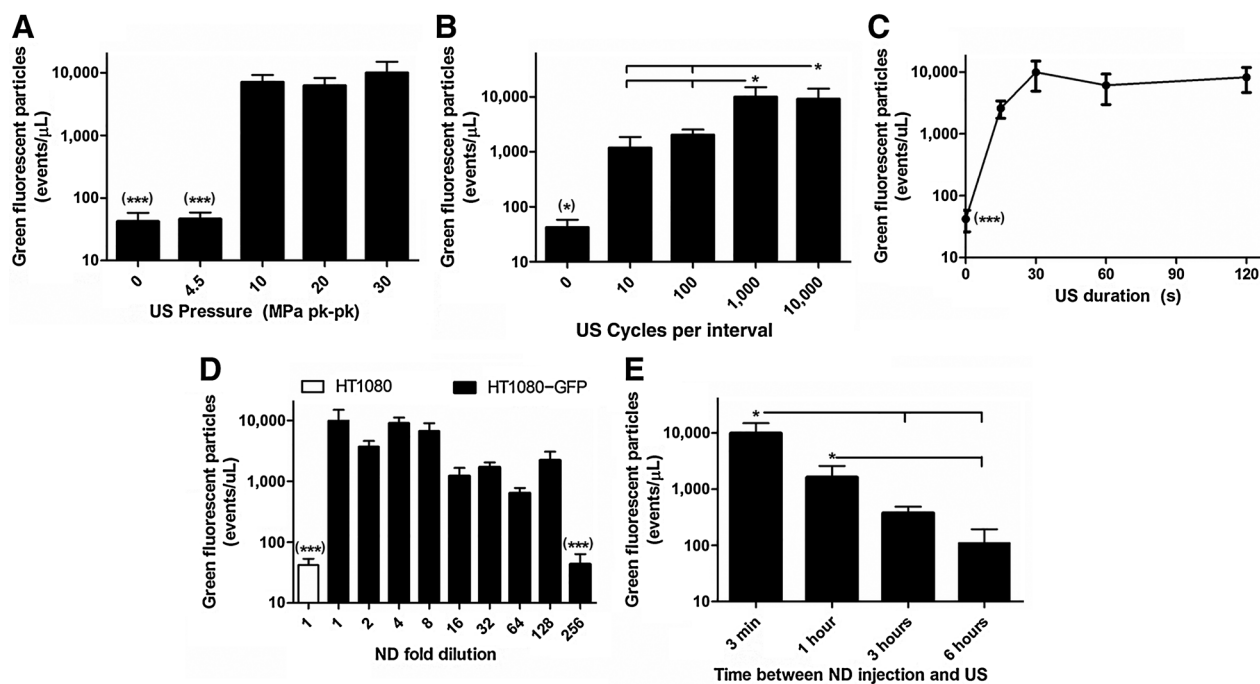
Sonication of HT1080 tumors with no GFP expression or sonication of the CAM without HT1080-GFP tumor cells resulted in no increase in green fluorescent EVs in the serum (Fig. 3B and C). The only conditions that caused a significant increase of green fluorescent EVs in the serum was sonication of HT1080-GFP tumors in embryos previously injected with nanodroplets (Fig. 3D and F), suggesting that both nanodroplets and ultrasound were necessary for EV release from tumors. Interestingly, some of the ultrasound-mediated released green fluorescent EVs displayed diameters >1,300 nm, which was much greater than the released particles observed from sonicated cultured cells (Figs. 2D and 3E). This may be due to the larger amount of ultrasound energy HT1080-GFP tumors were exposed to in the *in vivo* experiments. When performing similar *in vitro* (Supplementary Fig. S3A) and *in vivo* (Supplementary Fig. S3B) experiments described above but replacing nanodroplets with 0.51% microbubbles, ultrasound-mediated cancer-derived EV release significantly decreased and was similar to levels without ultrasound contrast agent. Unpurified and purified nanodroplets had similar EV release enhancing effects, suggesting that nanodroplets, and not the remaining microbubbles, were responsible for the observed ultrasound enhancing effects (Supplementary Fig. S3).

Optimizing ultrasound parameters for EV release from tumors

Various ultrasound and experimental parameters were individually altered to determine the optimal conditions for vesicle release from tumors *in vivo*. The lowest ultrasound pressure (pk-pk) tested causing significant EV release from HT1080-GFP tumors was 10 MPa (Fig. 4A). Higher pressures did not signifi-
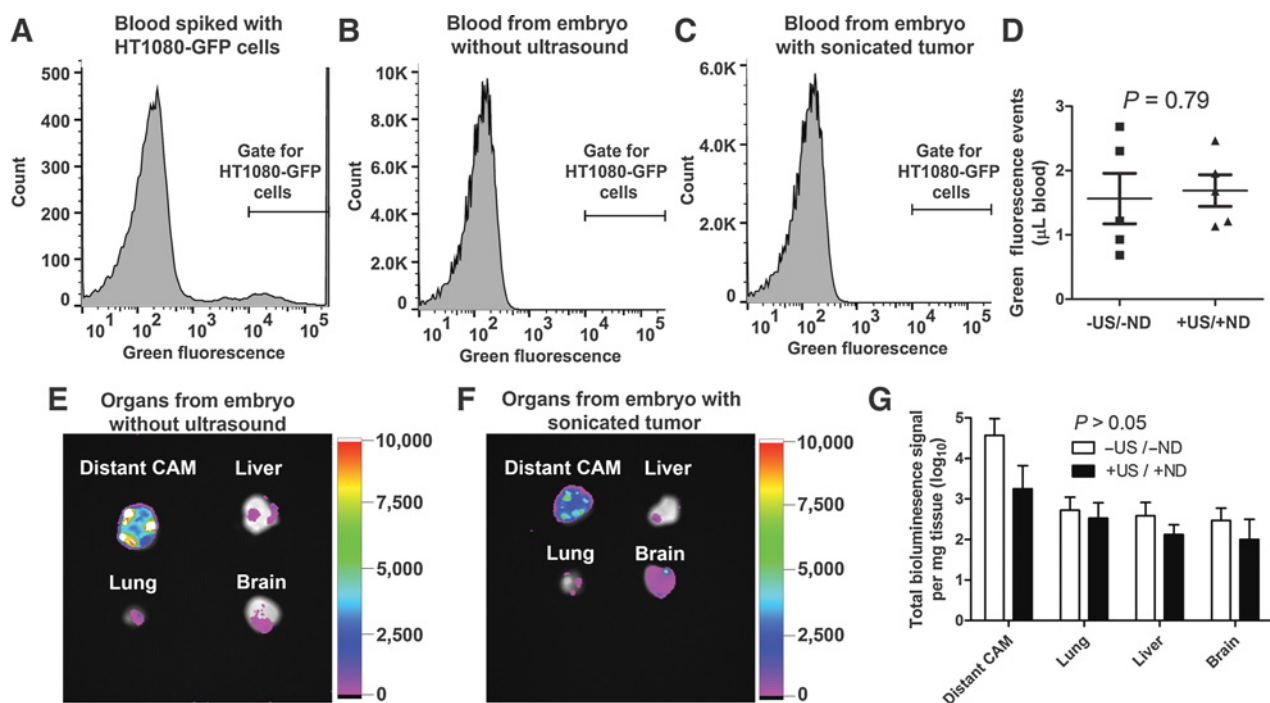
cantly increase EV release from tumors and had no effect on size of released EVs (Supplementary Fig. S4A). Increasing the number of transmitted ultrasound cycles per interval (burst) increased EV release up to 1,000 cycles, which displayed the maximum level of EV release (Fig. 4B). Varying ultrasound cycles per interval had no effect on size of released EVs (Supplementary Fig. S4B). The total duration of ultrasound exposure to the tumor affected EV release with the maximum effect observed at 30 seconds exposure (Fig. 4C). Interestingly, higher ultrasound durations caused the mean particle large angle light scatter to decrease, suggesting that longer sonication times increased the release of smaller particles (Supplementary Fig. S4C). Surprisingly, nanodroplets could be diluted 128-fold and still displayed relatively high levels of tumor EV release (Fig. 4D). These doses are comparable with clinically relevant dose recommendations for Definity microbubble contrast agents (27). Dilution of nanodroplets at 256-fold eliminated any observable tumor EV release. The time between nanodroplet intravenous injection and tumor sonication inversely affected tumor EV release (Fig. 4E) with the shortest time interval of 3 minutes displaying significantly greater tumor EV release than 3 or 6 hours ($P < 0.05$).

To determine the effect of ultrasound/nanodroplets on tumor cell viability, some HT1080-GFP tumor-bearing chicken embryos were intravenously injected with nanodroplets and had tumors exposed to ultrasound. Tumors were excised 24 hours post-sonication and TUNEL staining demonstrated that tumor regions outside the ultrasound focus remained viable, whereas apoptosis was detectable within the ultrasound focal zones (Supplementary Fig. S5).

Figure 4.
Determining the optimal ultrasound parameters and experimental conditions for detection of tumor vesicles in the serum. **A–E,** Green fluorescent particles in the serum of chicken embryos with HT1080-GFP tumors sonicated with varying ultrasound pressures (**A**), number of ultrasound cycles per interval (**B**), ultrasound duration (**C**), nanodroplet (ND) dilution for injection prior to tumor sonication (**D**), and time interval between nanodroplet injection and tumor sonication (**E**). For all panels, five chicken embryos were used per group and columns with * or *** were significantly different from indicated columns with $P < 0.05$ or 0.001, respectively. Asterisks with brackets were significantly different from all other groups without asterisks.

Figure 5.
Determining if ultrasound/nanodroplets increase the risk of metastasis. **A,** Flow cytometry histogram of green fluorescence levels of cells in chicken embryo blood spiked with HT1080-GFP cells. **B** and **C,** Flow cytometry histograms of green fluorescence levels of cells in blood of embryos bearing HT1080-GFP tumors without (**B**) or with (**C**) intravenous injection of nanodroplets and tumor sonication. **D,** Detectable green fluorescent events in chicken embryo blood with or without ultrasound/nanodroplet treatment (5 chicken embryos per group). Green fluorescent events can be derived from HT1080-GFP cells or background fluorescent particles in the sample. **E** and **F,** Bioluminescence (rainbow scale) and green fluorescence (grayscale) imaging of chicken embryo tissues from embryos without (**E**) or with (**F**) intravenous nanodroplet injection and tumor sonication 4 days before tissue dissection. Tissues include the CAM away from the primary tumor, liver, lung, and brain. **G,** Total bioluminescent signal per mg tissue from embryos with or without ultrasound/nanodroplet treatment (5 chicken embryos per group). No statistical differences were observed between groups ($P > 0.05$).

Tumor metastasis is not enhanced by ultrasound/nanodroplets

Using flow cytometry, we determined if sonication of tumors in embryos preinjected with nanodroplets caused increased circulating tumor cells in the blood. Compared with chicken embryos without ultrasound, embryos with tumors exposed to ultrasound had no significant increase in detectable HT1080-GFP cells in the blood (Fig. 5A–D). To determine if application of ultrasound/nanodroplets to tumors increased the tumors' metastatic potential, chicken embryos with HT1080-GFP tumors were given an intravenous injection of nanodroplets and tumors were sonicated. Four days after tumor sonication, tissues including the CAM (away from the tumor), liver, lung, and brain were dissected and imaged for green fluorescence and luciferase (Fig. 5E and F). In general, nanodroplet injection and tumor sonication caused decreased observed luciferase signal in tissues, although no significant differences were observed between groups (Fig. 5G). The results suggest that ultrasound/nanodroplets do not enhance the risk of tumor metastasis.

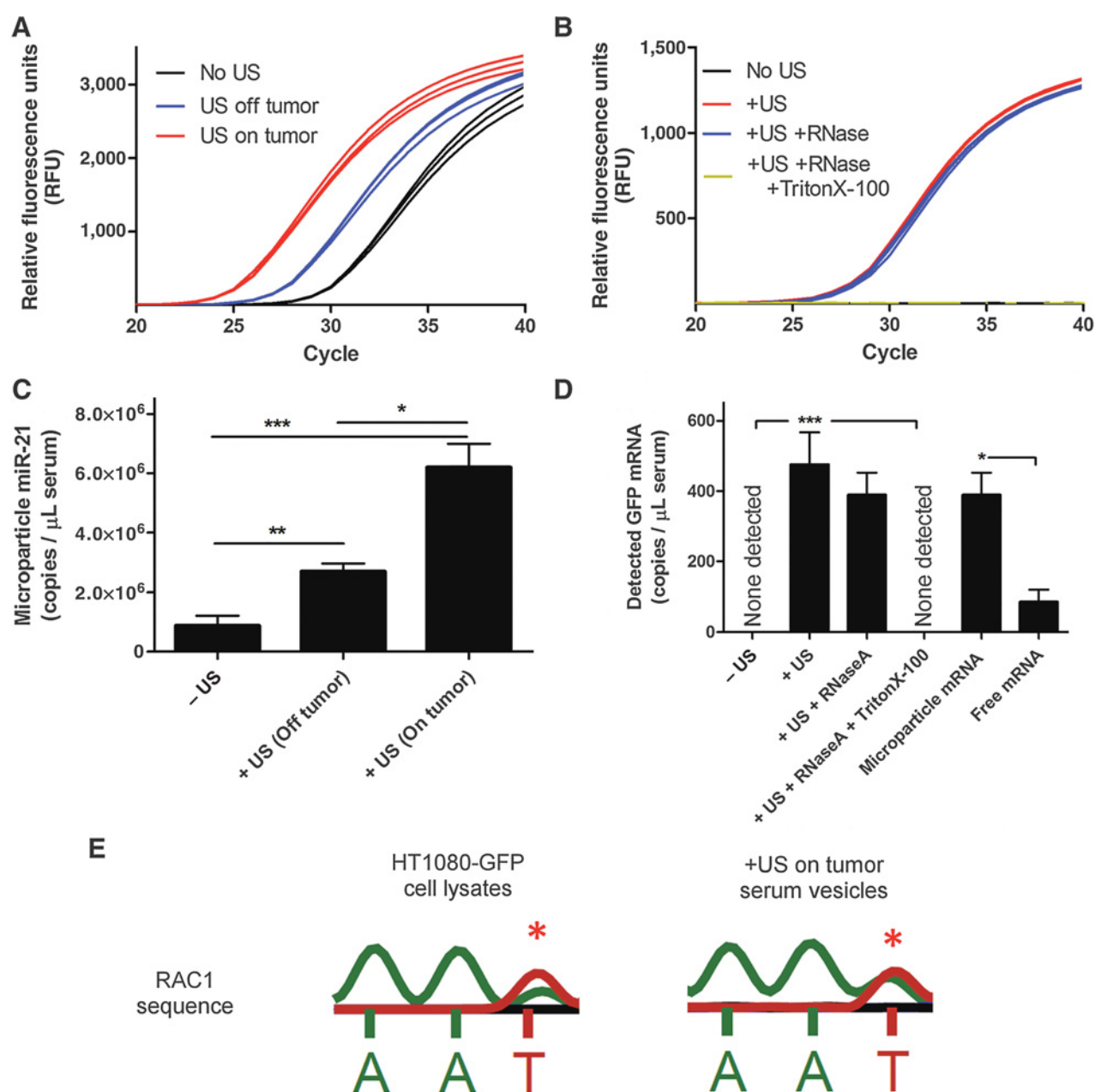## Enhanced detection of mRNA and miRNA in released tumor EVs

Using the optimal ultrasound conditions for tumor EV release, HT1080-GFP tumors were sonicated and the blood was analyzed for levels of miR21-5p and GFP mRNA. miR21-5p is an oncomir known to target a variety of tumor suppressor genes and to be up-regulated in several metastatic cancers (28, 29). Serum EVs were isolated by centrifugation, which allowed discrimination of free and EV-associated miRNAs. miR21-5p from EVs was present in serum of nonsonicated embryos at 880,000 copies per µL of serum (Fig. 6A and C). Ultrasound off or on tumors increased EV miR21-5p levels in serum three- and seven-fold, respectively, compared with nonsonicated tumors. miR21-5p is present in chicken cells, which likely explains the increase in miR21-5p when sonicating off of tumors. Compared with ultrasound off of tumors, ultrasound on tumors significantly increased EV miR21-5p levels in serum by 2.3-fold ($P < 0.05$, Fig. 6B). Serum miR21-5p levels were approximately 95% free and 5% in EVs regardless of ultrasound application. GFP mRNA was undetectable in the blood without tumor sonication but was detectable at 480 copies per µL of serum after tumor sonication (Fig. 6B and D). EV-associated GFP mRNA, determined by incubating samples in RNaseA, which degraded mRNA outside of EVs, represented 82% of detectable GFP mRNA (Fig. 6D).

Enhanced detection of tumor-specific mutations in released EVs

To assess whether EV mRNA released from tumors could be used for identification of cancer genetic signatures, we sought to detect the N92I RAC1 mutation in HT1080-GFP cells, which conveys increased tumorigenicity (30). EV-associated RAC1 mRNA was only detectable in serum samples from embryos bearing HT1080-GFP tumors that were exposed to nanodroplets and ultrasound. EV-derived RAC1 mRNA contained the N92I

Paproski et al.

Figure 6.
Analysis of RNA released from sonicated HT1080-GFP tumors. **A** and **B,** Fluorescence of real-time PCR samples of serum vesicle RNA (**A**) or total serum RNA (**B**) using miR21-5p TaqMan probe and primers (**A**) or GFP primers (**B**). **C,** Vesicle miR21-5p levels in serum of chicken embryos injected with nanodroplets with or without ultrasound on or off HT1080-GFP tumors (3–5 chicken embryos per group). **D,** Serum GFP mRNA levels in chicken embryos injected with nanodroplets with or without ultrasound on HT1080-GFP tumors. Serum samples were incubated with or without RNaseA and Triton X-100 to determine vesicle GFP mRNA levels (3 chicken embryos per group). **E,** N92I RAC1 mutation detected in mRNA from HT1080+GFP cell lysates and serum vesicles of embryos bearing HT1080+GFP tumors that were exposed to ultrasound. For **A–D**, columns with *, **, or *** are significantly different from indicated columns with $P < 0.05$, 0.01, or 0.001, respectively.

mutation, which was detectable in cultured HT1080-GFP cells (Fig. 6E). In addition, PCR amplification of fragments encompassing heterozygous mutations reported in the catalogue of somatic mutations in cancer (COSMIC), followed by low-pass deep sequencing, allowed the identification of 13 mutations in the HT1080 genome (Supplementary Table S1). The data suggest that ultrasound released EVs contain genetic information capable

of profiling tumor-specific mutations, which can predict tumor aggressiveness.

Enhanced detection of tumor genomic DNA in released EVs

We then determined whether the application of focused ultrasound in the presence of nanodroplets could enhance the detection of tumor genomic DNA circulating in the blood.

Next-generation sequencing libraries were constructed from DNA isolated from serum of chicken embryos bearing larger HT1080-GFP tumors (2–5 mm) or smaller HEp3-GFP tumors (1–2 mm), with or without ultrasound exposure and injection of nanodroplets. Nanodroplets/ultrasound exposure to the HEp3 and HT1080-GFP tumors increased the number of human DNA sequence reads in serum by 16- and 102-fold, respectively, compared with embryos without tumor sonication (Fig. 7A and B) with apparent uniform coverage of the entire tumor genome for HT1080 tumors (Fig. 7C). These encouraging results indicate that nanodroplets and ultrasound can significantly enhance the levels of tumor-derived DNA in the blood, even in very small lesions.
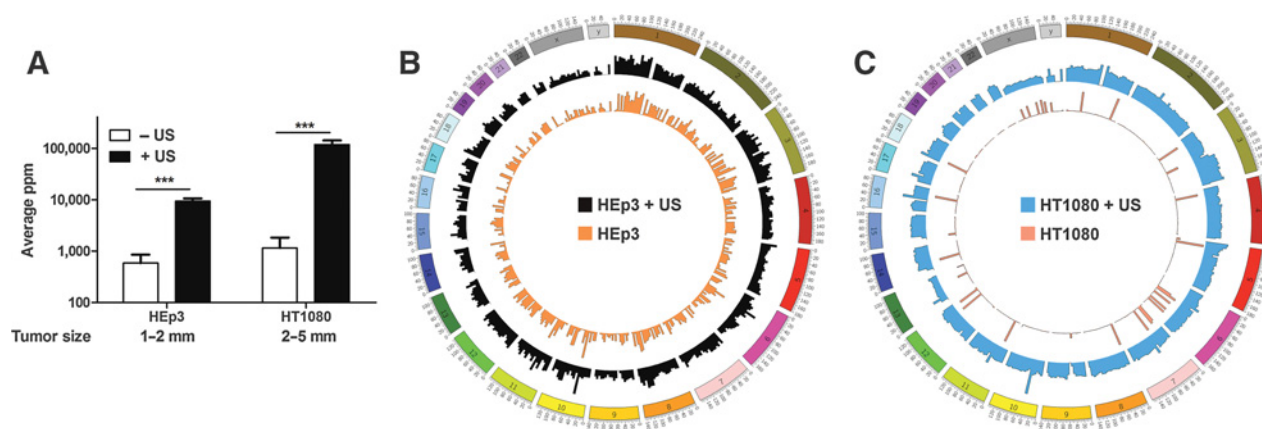
Discussion

This study provides evidence that focused ultrasound in the presence of nanodroplets can enhance the release and detection of EVs and their associated biomarkers from tumors into the blood. Given that high-intensity focused ultrasound can be focused in regions approximately $5 \times 1 \times 1$ mm, target tissues can receive ultrasound exposure in precise regions to stimulate localized EV release into the bloodstream. Blood samples can be acquired and compared pre-/postsonication to interrogate biomarker levels in precise regions of interest with baseline biomarker levels determined for each patient. This would be ideal for biomarkers with significant interpatient variability including PSA for prostate cancer (31).

Although our in vitro data suggested that ultrasound and nanodroplets caused minimal cell death, our in vivo data demonstrated apoptosis within small tumor regions corresponding to cells within ultrasound focal zones. This discrepancy is likely due to differences in (i) total ultrasound energy applied to cells, and (ii) the cell environment (i.e., 2D cultures with abundant nutrients vs. 3D tissues requiring blood vessels

for nutrients). High pressure ultrasound, especially with ultrasound contrast agents, can damage blood vessels and impair their function, potentially increasing cell death of nearby cells (32, 33). The side effect of tumor cell death may be considered beneficial, although this may restrict our diagnostic technique to known tumor locations. Focused ultrasound will be necessary to minimize the toxicity of this technique to small regions of interest.

Deeply focused ultrasound minimizes skin exposure to ultrasound pressures necessary for microbubble destruction and likely eliminating the risk of infection. By comparison, biopsy needles physically disrupt all tissues from the skin to the target biopsy site, significantly increasing the risk of infection. Such wide-scale physical disruption of tissue may explain why biopsies have been observed to increase the risk of metastasis (34). Interestingly, ultrasound exposure to cultured PC3 prostate cancer cells incubated with microbubbles have demonstrated reduced cell migration and invasion with reduced MMP-2 and MMP-9 expression (35). In another study, metastasis was reduced in mice bearing breast 4T1 tumors when mice were injected with microbubbles and had tumors sonicated (36). These results as well as our own suggest that tumor sonication with ultrasound contrast agents is more likely to inhibit rather than promote tumor metastasis.

Although physical biopsies have some risks to patients, they have proven effective for characterizing different malignancies and provide valuable clinical information that influences clinical decisions. Biopsies provide tumor samples with intact physical architecture that cannot be acquired with ultrasound and blood samples. We do not propose that nanodroplets and ultrasound should necessarily supplant traditional biopsy methods. Instead, we believe nanodroplets and ultrasound may provide additional tumor-derived material when traditional biopsy methods may not be appropriate. Sonication of tumors for biomarker release may also be useful for research studies if longitudinal repeat

Figure 7.
Whole genome sequencing of DNA in serum from chicken embryos bearing HEp3 or HT1080 tumors. **A,** Relative abundance of human reads in genomic libraries derived from serum of chicken embryos harboring HEp3-GFP or HT1080-GFP tumors without or with ultrasound exposure. Reads that aligned to the Gallus gallus genome (galGal3) were removed and the remaining reads were aligned against the human genome (hg19) with Bowtie2, using default parameters. **B** and **C,** Genome coverage plots generated from genomic libraries from serum DNA from chicken embryos harboring either HEp3 (**B**) or HT1080 (**C**) tumors, with or without ultrasound applied (number of libraries: HEp3+US = 4, HEp3 = 2, HT1080+US = 6, HT1080 = 4). In all cases, sequences from individual libraries in each group were pooled, mapped along the human genome, and then binned into windows of 7.5 Megabases, with bar heights representing normalized sequence counts in specific genomic locations (normalization was done dividing each count by the sum of total human and chicken reads mapped to the respective genome). Columns with *** were significantly different from indicated columns with $P < 0.001$.

tumor biopsies are too invasive. In addition, biomarkers could be liberated from different focal regions of tumors for analyzing tumor heterogeneity.

Intravenous injection of nanodroplets was required for detection of tumor-derived vesicles after tumor sonication. Given that vesicle release was greatest with the shortest time interval between nanodroplet injection and tumor sonication (3 minutes), the vast majority of the nanodroplets would have been present within the blood vessels during this time. This suggests that vesicle release from tumors is maximized when nanodroplets are destroyed near endothelial cells. Ultrasound-mediated microbubble destruction in the blood vessels of the chorioallantoic membrane has previously been shown to increase blood vessel permeabilization, suggesting that this may be an important mechanism for how tumor vesicles entered the vasculature (33).

One major limitation of our study is the difference in cancer vesicle/biomarker detection in our experiments and in the clinic. We use GFP expressing tumors to easily identify cancer vesicles in the serum, which does not translate in the clinic. Additionally, we used human-specific primers for detection and sequencing of HT1080-GFP tumor RAC1 mRNA. In the clinic, tumor-specific gene primers cannot necessarily be designed. To identify and characterize ultrasound-mediated mRNA release from tumors, tumor-derived vesicles could be purified using affinity columns or immuno-magnetic methods for cell surface markers present specifically on tumor cells. These purified tumor vesicles from the serum could then be analyzed to determine tumor genetics as previously demonstrated (37).

Analyzing circulating tumor DNA (ctDNA) is a potentially powerful diagnostic technique for profiling tumor genetics (38, 39). Unfortunately, ctDNA levels vary greatly between patients with some patients exhibiting no detectable ctDNA. Much of the ctDNA is believed to be derived from circulating tumor cells, suggesting that analysis of ctDNA would primarily be useful in patients with advanced metastatic disease. Given that chicken embryos bearing HT1080-GFP tumors had minimal ctDNA before ultrasound but >100-fold increased levels after ultrasound, our nanodroplet/ultrasound-based technique may allow genomic characterization of localized tumors that is ideal, because tumor aggressiveness should be determined before cancers metastasize while they are still typically curable.

To our knowledge, this is the first study to determine that nanodroplets and ultrasound can stimulate vesicle release from tumor cells that can be detected in the serum. The released vesicles contained tumor-derived protein/nucleic acid biomarkers with tumor-specific mutations allowing characterization of tumor phenotype including aggressiveness. Future studies opti-

mizing this procedure in larger animal models with longer longitudinal safety studies are warranted. This diagnostic technique may provide clinically relevant tumor information for situations where (repeat) needle biopsies are not appropriate due to health risks to patients. Our findings suggest a new paradigm and path forward for biomarker research with the vision that radiographically identified lesions could be sonicated with image-guidance to stimulate release of biomarker-loaded vesicles for molecular profiling of tumors.

Disclosure of Potential Conflicts of Interest

No potential conflicts of interest were disclosed.

Authors' Contributions

Conception and design: R.J. Paproski, J.D. Lewis, R.J. Zemp
Development of methodology: R.J. Paproski, J.D. Lewis, R.J. Zemp
Acquisition of data (provided animals, acquired and managed patients, provided facilities, etc.): R.J. Paproski, J. Jovel, G.K.-S. Wong, J.D. Lewis
Analysis and interpretation of data (e.g., statistical analysis, biostatistics, computational analysis): R.J. Paproski, J. Jovel, J.D. Lewis, R.J. Zemp
Writing, review, and/or revision of the manuscript: R.J. Paproski, J. Jovel, G.K.-S. Wong, J.D. Lewis, R.J. Zemp
Administrative, technical, or material support (i.e., reporting or organizing data, constructing databases): J. Jovel, R.J. Zemp
Study supervision: J.D. Lewis, R.J. Zemp

References

1. Miyamoto DT, Sequist LV, Lee RJ. Circulating tumour cells-monitoring treatment response in prostate cancer. Nat Rev Clin Oncol 2014; 11:401–12.
2. Kharaziha P, Ceder S, Li Q, Panaretakis T. Tumor cell-derived exosomes: a message in a bottle. Biochim Biophys Acta 2012;1826:103–11.
3. Nawaz M, Camussi G, Valadi H, Nazarenko I, Ekstrom K, Wang XQ, et al. The emerging role of extracellular vesicles as biomarkers for urogenital cancers. Nat Rev Urol 2014;11:688–701.
4. Valadi H, Ekstrom K, Bossios A, Sjostrand M, Lee JJ, Lotvall JO. Exosome-mediated transfer of mRNAs and microRNAs is a novel mechanism of genetic exchange between cells. Nat Cell Biol 2007;9:654–U72.
5. Lohr JG, Adalsteinsson VA, Cibulskis K, Choudhury AD, Rosenberg M, Cruz-Gordillo P, et al. Whole-exome sequencing of circulating tumor cells provides a window into metastatic prostate cancer. Nat Biotechnol 2014; 32:479–484.
6. Phillips R. Prostate cancer: probing progression in circulating tumour cells. Nat Rev Urol 2014;11:486.
7. EL Andaloussi S, Mager I, Breakefield XO, Wood MJ. Extracellular vesicles: biology and emerging therapeutic opportunities. Nat Rev Drug Discov 2013;12:347–57.
8. Ginestra A, La Placa MD, Saladino F, Cassara D, Nagase H, Vittorelli ML. The amount and proteolytic content of vesicles shed by human cancer cell

lines correlates with their in vitro invasiveness. Anticancer Res 1998;18:3433–7.

9. D'Souza-Schorey C, Clancy JW. Tumor-derived microvesicles: shedding light on novel microenvironment modulators and prospective cancer biomarkers. Genes Dev 2012;26:1287–99.

10. Choi DS, Lee J, Go G, Kim YK, Gho YS. Circulating extracellular vesicles in cancer diagnosis and monitoring: an appraisal of clinical potential. Mol Diagn Ther 2013;17:265–71.

11. Zocco D, Ferruzzi P, Cappello F, Kuo WP, Fais S. Extracellular vesicles as shuttles of tumor biomarkers and anti-tumor drugs. Front Oncol 2014;4:267.

12. Melo SA, Luecke LB, Kahlert C, Fernandez AF, Gammon ST, Kaye J, et al. Glypican-1 identifies cancer exosomes and detects early pancreatic cancer. Nature 2015;523:177–82.

13. Leyten GH, Hessels D, Jannink SA, Smit FP, de Jong H, Cornel EB, et al. Prospective multicentre evaluation of PCA3 and TMPRSS2-ERG gene fusions as diagnostic and prognostic urinary biomarkers for prostate cancer. Eur Urol 2014;65:534–42.

14. D'Souza AL, Tseng JR, Pauly KB, Guccione S, Rosenberg J, Gambhir SS, et al. A strategy for blood biomarker amplification and localization using ultrasound. Proc Natl Acad Sci U S A 2009;106:17152–7.

15. Forbrich A, Paproski R, Hitt M, Zemp R. Microbubble-enhanced ultrasound liberation of mRNA biomarkers in vitro. Ultrasound Med Biol 2013;39:1087–93.

16. Paproski RJ, Forbrich A, Hitt M, Zemp R. RNA biomarker release with ultrasound and phase-change nanodroplets. Ultrasound Med Biol 2014;40:1847–56.

17. Prentice P, Cuschieri A, Dholakia K, Prausnitz M, Campbell P. Membrane disruption by optically controlled microbubble cavitation. Nat Phys 2005;1:107–10.

18. Qin S, Caskey CF, Ferrara KW. Ultrasound contrast microbubbles in imaging and therapy: physical principles and engineering. Phys Med Biol 2009;54:R27–57.

19. Rapoport N. Phase-shift, stimuli-responsive perfluorocarbon nanodroplets for drug delivery to cancer. Wiley Interdiscip Rev Nanomed Nanobiotechnol 2012;4:492–510.

20. Sheeran PS, Luois S, Dayton PA, Matsunaga TO. Formulation and acoustic studies of a new phase-shift agent for diagnostic and therapeutic ultrasound. Langmuir 2011;27:10412–20.

21. Qiu Y, Luo Y, Zhang Y, Cui W, Zhang D, Wu J, et al. The correlation between acoustic cavitation and sonoporation involved in ultrasound-mediated DNA transfection with polyethylenimine (PEI) invitro. J Control Release 2010;145:40–8.

22. Cho CF, Ablack A, Leong HS, Zijlstra A, Lewis J. Evaluation of nanoparticle uptake in tumors in real time using intravital imaging. J Vis Exp 2011;52. Doi:10.3791/2808.

23. Kain KH, Miller JW, Jones-Paris CR, Thomason RT, Lewis JD, Bader DM, et al. The chick embryo as an expanding experimental model for cancer and cardiovascular research. Dev Dyn 2014;243:216–28.

24. Leong HS, Steinmetz NF, Ablack A, Destito G, Zijlstra A, Stuhlmann H, et al. Intravital imaging of embryonic and tumor neovasculature using viral nanoparticles. Nat Protoc 2010;5:1406–17.

25. Palmer TD, Martinez CH, Vasquez C, Hebron KE, Jones-Paris C, Arnold SA, et al. Integrin-free tetraspanin CD151 can inhibit tumor cell motility upon clustering and is a clinical indicator of prostate cancer progression. Cancer Res 2014;74:173–87.

26. Roncella S, Ferro P, Bacigalupo B, Pronzato P, Tognoni A, Falco E, et al. Human mammaglobin mRNA is a reliable molecular marker for detecting occult breast cancer cells in peripheral blood. J Exp Clin Cancer Res 2005;24:265–71.

27. Kitzman DW, Goldman ME, Gillam LD, Cohen JL, Aurigemma GP, Gottdiener JS. Efficacy and safety of the novel ultrasound contrast agent perflutren (definity) in patients with suboptimal baseline left ventricular echocardiographic images. Am J Cardiol 2000;86:669–74.

28. Buscaglia LE, Li Y. Apoptosis and the target genes of microRNA-21. Chin J Cancer 2011;30:371–80.

29. Wang W, Li J, Zhu W, Gao C, Jiang R, Li W, et al. MicroRNA-21 and the clinical outcomes of various carcinomas: a systematic review and meta-analysis. BMC Cancer 2014;14:819.

30. Kawazu M, Ueno T, Kontani K, Ogita Y, Ando M, Fukumura K, et al. Transforming mutations of RAC guanosine triphosphatases in human cancers. Proc Natl Acad Sci U S A 2013;110:3029–34.

31. Litchfield MJ, Cumming RG, Smith DP, Naganathan V, Le Couteur DG, Waite LM, et al. Prostate-specific antigen levels in men aged 70 years and over: findings from the CHAMP study. Med J Aust 2012;196:395–8.

32. Al-Mahrouki AA, Iradji S, Tran WT, Czarnota GJ. Cellular characterization of ultrasound-stimulated microbubble radiation enhancement in a prostate cancer xenograft model. Dis Model Mech 2014;7:363–72.

33. Stieger SM, Caskey CF, Adamson RH, Qin S, Curry FR, Wisner ER, et al. Enhancement of vascular permeability with low-frequency contrast-enhanced ultrasound in the chorioallantoic membrane model. Radiology 2007;243:112–21.

34. Mathenge EG, Dean CA, Clements D, Vaghar-Kashani A, Photopoulos S, Coyle KM, et al. Core needle biopsy of breast cancer tumors increases distant metastases in a mouse model. Neoplasia 2014;16:950–60.

35. Wei C, Bai WK, Wang Y, Hu B. Combined treatment of PC-3 cells with ultrasound and microbubbles suppresses invasion and migration. Oncol Lett 2014;8:1372–76.

36. Chen YL, Wang CY, Yang FY, Wang BS, Chen JY, Lin LT, et al. Synergistic effects of glycated chitosan with high-intensity focused ultrasound on suppression of metastases in a syngeneic breast tumor model. Cell Death Dis 2014;5:e1178.

37. Shao H, Chung J, Balaj L, Charest A, Bigner DD, Carter BS, et al. Protein typing of circulating microvesicles allows real-time monitoring of glioblastoma therapy. Nat Med 2012;18:1835–40.

38. Crowley E, Di Nicolantonio F, Loupakis F, Bardelli A. Liquid biopsy: monitoring cancer-genetics in the blood. Nat Rev Clin Oncol 2013;10:472–84.

39. Schwarzenbach H, Hoon DS, Pantel K. Cell-free nucleic acids as biomarkers in cancer patients. Nat Rev Cancer 2011;11:426–37.

Cancer Research

The Journal of Cancer Research (1916–1930) | The American Journal of Cancer (1931–1940)

AACR American Association for Cancer Research

Enhanced Detection of Cancer Biomarkers in Blood-Borne Extracellular Vesicles Using Nanodroplets and Focused Ultrasound

Robert J. Paproski, Juan Jovel, Gane Ka-Shu Wong, et al.

Updated version	Access the most recent version of this article at: doi:10.1158/0008-5472.CAN-15-3231
Supplementary Material	Access the most recent supplemental material at: http://cancerres.aacrjournals.org/content/suppl/2016/10/28/0008-5472.CAN-15-3231.DC1

Cited articles	This article cites 38 articles, 5 of which you can access for free at: http://cancerres.aacrjournals.org/content/77/1/3.full.html#ref-list-1

E-mail alerts	Sign up to receive free email-alerts related to this article or journal.
Reprints and Subscriptions	To order reprints of this article or to subscribe to the journal, contact the AACR Publications Department at pubs@aacr.org.
Permissions	To request permission to re-use all or part of this article, contact the AACR Publications Department at permissions@aacr.org.